



HAL
open science

Systemic Analysis of the Spatiotemporal Changes in Multi-Species Electroactive Biofilms to Clarify the Gradual Decline of Current Generation in Microbial Anodes

Lucila Martinez Ostormujof, Sébastien Teychené, Wafa Achouak, Sylvain Fochesato, Mohamed Bakarat, Isaac Rodriguez-Ruiz, Alain Bergel, Benjamin Erable

► **To cite this version:**

Lucila Martinez Ostormujof, Sébastien Teychené, Wafa Achouak, Sylvain Fochesato, Mohamed Bakarat, et al.. Systemic Analysis of the Spatiotemporal Changes in Multi-Species Electroactive Biofilms to Clarify the Gradual Decline of Current Generation in Microbial Anodes. *ChemElectroChem*, 2023, 10 (9), pp.1-13. 10.1002/celec.202201135 . hal-04295622

HAL Id: hal-04295622

<https://hal.science/hal-04295622>

Submitted on 20 Nov 2023

HAL is a multi-disciplinary open access archive for the deposit and dissemination of scientific research documents, whether they are published or not. The documents may come from teaching and research institutions in France or abroad, or from public or private research centers.

L'archive ouverte pluridisciplinaire **HAL**, est destinée au dépôt et à la diffusion de documents scientifiques de niveau recherche, publiés ou non, émanant des établissements d'enseignement et de recherche français ou étrangers, des laboratoires publics ou privés.

Special
Collection

Systemic Analysis of the Spatiotemporal Changes in Multi-Species Electroactive Biofilms to Clarify the Gradual Decline of Current Generation in Microbial Anodes

Lucila Martinez Ostormujof,^[a] Sébastien Teychené,^[a] Wafa Achouak,^[b] Sylvain Fochesato,^[b] Mohamed Bakarat,^[b] Isaac Rodriguez-Ruiz,^[a] Alain Bergel,^[a] and Benjamin Erable^{*[a]}

The decrease in the electrochemical activity of multi-species microbial anodes in bioelectrochemical systems is the main bottleneck to overcome for bringing these technologies one-step closer to the industrialization stage. In this study, micro-sized stainless steel electrodes were implemented to investigate the distinctive electrochemical behavior of salt marsh electroactive biofilms (EABs). Four main temporal stages of biocolonization and electrochemical activity were thoroughly described. Maximum biofilm growth rate, high viability and high extracellular protein matrix content favored the increasing electro-

chemical activity of the EAB up to its maximum current peak. Then, when gradual fall in current became irreversible, biofilm growth rate decreased together with dead cells accumulation and an increase for extracellular polysaccharides. In addition, analyses of microbial populations showed a shift from *Marinobacterium* spp. to *Desulfuromonas* spp. These findings suggest a chemical and microbial temporal evolution of the EAB, which can be directly correlated to the electrochemical performance of the bioanode.

Introduction

Bioelectrochemical systems (BES) are unique environmental technologies with a wide range of applications today: energy conversion, wastewater treatment, soil remediation, electro-fermentation, bioelectrosynthesis of energy carriers and chemical building blocks, and biosensors.^[1–3] Their ability to transform organic waste streams into energy positions BES as a promising technology for a circular bioeconomy,^[4] a reduction of the environmental footprint of processes and an environmental biorefinery strategy. The operating principle of BES is based on the central operation of electroactive biofilm (EAB) which catalyzes bioelectrochemical reactions of mass and energy transformation. In the specific case of the bioanode, the electroactive microbial biofilm catalyzes the oxidation of various organic substances to produce an electric current that is

captured by the anode. Microbial bioanodes thus represent the functional core of BES.^[5]


However, despite all the strategic, economic and ecological advantages and opportunities offered by BES, their implementation is still at the laboratory scale, even though these technologies were first demonstrated more than 20 years ago.^[6,7] The issue of scaling-up of BES or the low current densities supported are widely recognized obstacles to the industrial democratization of these technologies.^[8,9] Also, the loss of electrochemical activity on microbial bioanodes seems to be the main barrier to overcome in order to improve the long-term sustainability of BES. A large number of studies (Table S1) have indeed documented anode current densities with mixed electroactive biofilms that severely drop after a few days or tens of days of operation, sometimes even losing more than 50% of their maximum performance. Among the possible causes reported to explain the loss of electrochemical activity of microbial bioanodes, it is acknowledged:


- (i) A restrictive active biofilm thickness: this means that the biofilm is electrochemically active at low thicknesses and then its activity gradually decreases as the biofilm grows.^[10] This phenomenon can be explained by a change in the predominant electron transfer mechanism when the biofilm reaches a threshold thickness^[11] or limitations in the respiration rates of the biofilm when it is distant from the electrode.^[12,13] This has been mainly studied using pure strain bacteria of *Geobacter Sulfurreducens*.
- (ii) Nutrient and/or substrate depletion in the anolyte, and/or generation of metabolic by-products over time, and/or the presence of oxidized chemical compounds that may inhibit microbial growth or compete with the electrode as an electron acceptor.^[14] Working in fed-batch mode when current generation in the bioanode decreases showed


[a] L. Martinez Ostormujof, Dr. S. Teychené, Dr. I. Rodriguez-Ruiz, Dr. A. Bergel, Dr. B. Erable

Laboratoire de Génie Chimique
Université de Toulouse, CNRS, INPT, UPS
4 allée Emile Monso, BP 94234, 31432 Toulouse (France)
E-mail: benjamin.erable@toulouse-inp.fr

[b] Dr. W. Achouak, S. Fochesato, M. Bakarat
Lab of Microbial Ecology of the Rhizosphere (LEMIRE)
BIAM, UMR 7265 CNRS-CEA-Aix Marseille University
CEA Cadarache
13115 Saint Paul lez Durance (France)

 Supporting information for this article is available on the WWW under <https://doi.org/10.1002/celc.202201135>

 An invited contribution to the Plamen Atanassov Festschrift

 © 2023 The Authors. ChemElectroChem published by Wiley-VCH GmbH. This is an open access article under the terms of the Creative Commons Attribution License, which permits use, distribution and reproduction in any medium, provided the original work is properly cited.

improvements in the electroactivity of the EAB. In addition, the use of artificial wastewater allows the composition of the anolyte to be controlled, thus avoiding deficiencies and the contribution of possible soluble electron acceptors in the liquid medium.^[15]

- (iii) Increasing spatial, microbial and chemical heterogeneity within the biofilm, creating inactive regions that do not contribute to electrochemical activity. This is mainly caused by nutrient and substrate gradients between the liquid bulk and the internal body of the biofilm,^[16] variation in redox potential in the biofilm matrix as the distance between the bacterial cells and the electrode increases,^[17,18] as well as to the accumulation of metabolites resulting from bioelectrochemical or only biochemical reactions. Examples include local acidification due to proton production during the bioelectrochemical oxidation of simple substrates^[19,20] or massive production of Volatile Fatty Acids (VFA) during anaerobic biochemical degradation of complex organic compounds during the acidogenic fermentation.^[21,22]
- (iv) Excessive accumulation of extracellular polysaccharides in the exopolymeric biofilm matrix. Studies with pure *Geobacter Soli* strains^[23] and mixed population inoculums enriched with *Geobacter*^[24,25] showed a negative correlation between increased polysaccharide and current production, due to their insulating nature.

In sum, there are a number of well-founded explanations or theoretical hypotheses justifying why the electrochemical activity of anodic biofilms is depleted over time or during the maturation of the biofilm on the electrode. Most of these justifications or theories result from studies based on simplified experimental systems involving pure model electroactive bacterial strains such as *Geobacter Sulfurreducens* or *Shewanella Oneidensis*. However, the use of a mixed community of microorganisms (a multi-species consortium) induces an increased complexity where the mechanisms of biofilm formation are different from one microbial species to another, where electroactive bacteria coexist with non-electroactive bacteria, and where the mechanisms of electron transfer and polymer matrix synthesis (EPS) can be significantly diversified within the biofilm. This makes multi-species electroactive biofilms a very complex object of investigation, especially when looking at its dynamics over long-time scales.

Until now, the usual methodological approaches to investigate anodic biofilms of microbial bioanodes are classically conducted at the global scale of the biofilm, by implementing macroelectrodes in BES of several milliliters to several liters. With these configurations, the control of constant physicochemical conditions at the anode-liquid bulk interface is difficult to guarantee. Also, the use of non-planar electrodes such as felts, cloths, brushes or any other geometry with minimal porosity or roughness results in potential gradients that are not ideal for conducting fundamental studies.^[26] Structural analyses of biofilms are mostly performed after sampling the bioanodes in BES and after post-treatments (collecting, cleaning, fixing, specific labelling, dehydration...) that heavily affect the native configurations and properties of the biofilms. These analyses,

whether chemical, microscopic, genetic or functional, are generally carried out at a single time point in the experiment, usually at the end of the run. This non-consideration of the dynamics of the biofilm as an evolutive living system, where its properties evolve temporally and spatially, contributes to a great loss of valuable information in relation to its electroactivity.

The integration of wire-based microelectrodes in BES allows, on the contrary, to work with physicochemical conditions and theoretically homogeneous potentials at the microelectrode – bulk liquid interface, which are more ideal conditions for applying electroanalytical methods. Also the mass transfer is considerably less limited in the periphery of the wire microelectrodes.^[27] This property is valid both for promoting the formation of homogeneous anodic electroactive biofilms,^[28] as well as for post-treating the biofilms homogeneously and rapidly with aqueous marking solutions (dye, DNA probes, fluorescent substances) or cleaning solutions.

In the present study, we investigated the correlation between the electrochemical activity of multi-species microbial bioanodes and the spatio-temporal dynamics of biofilm formation. For this purpose, stainless steel microelectrodes were implemented as anode materials in BES. Electroactive salt marsh biofilms were formed under constant polarization on these stainless steel microelectrodes. Biofilm growth, microbial viability, EPS composition, and bacterial species abundance were determined on the biofilm volume at four key stages of microelectrode biocolonisation. The use of a fed-batch feeding system was also applied in stages where electrochemical activity falls with the objective to recover the loss of electroactivity observed over the long term. We aim to elucidate the process change that contributes to the loss of performance of the microbial anodes for the future definition of strategies that could improve their long-term durability.

Results and Discussion

Microelectrodes are a suitable tool to study the mechanisms of biofilm formation

The electroactivity of multi-species EABs has been shown to gradually deplete after a few tens of days of BES operation (Table S1), certainly as the chemical and biological composition, biofilm thickness and cell viability evolve on the electrode surface. The primary objective of our work was to reproduce this dynamic decline in the electroactivity of multispecies EABs on microelectrodes. Microelectrodes offer several advantages: (i) the electroanalytical conditions are more precisely controlled, (ii) the EABs implant on their surface in a more homogeneous form,^[28] and (iii) the post-treatment and subsequent analyses, such as imaging, are more simplified and immediate. Salt marsh electroactive biofilms from hypersalinity sediments were formed in duplicate under constant polarization of 0.1 V/SCE for a total time of 55 days. This potential value was applied according to similar experiments performed in the last 10 years with salt marsh inoculum and a concentration of 45 gL⁻¹ of NaCl.^[29] At

this applied potential, the 316 L stainless steel material is stable and protected from corrosion in a saline or marine environment. Actually, negative controls carried out without microbial inocula or with inactive inocula have shown that the current can remain null for several tens of days. The generation of current related to the establishment of an electroactive biofilm is monitored over time by chronoamperometry. After the polarization was stopped, the biocolonization and physical structure of biofilms was observed under epifluorescence microscopy and scanning electron microscopy.

The four stages shown in Figure 1A can be described as follows:

Stage I: Initial lag phase: After inoculation, electroactive bacteria present in the microbial salt marsh consortium needs to adapt to the anoxic and highly saline environment, and to the 40 mM of acetate in the synthetic medium. In this period, current is not produced in the anode. Stage I was described for the time when current reaches 0.1 A m^{-2} as adapted from a previous study.^[30] In our case, duplicates reached that value at a time of 5.9 ± 0.5 days.

Stage II: Maximum current production phase: Later, current increased sharply, reaching a maximum current density value. This peak is known as J_{max} and for the two duplicates it corresponded to $J_{\text{max}} = 10.0 \pm 0.5 \text{ A m}^{-2}$.

Stage III: Current decrease phase: Even if the concentration of electron donor was regularly monitored and kept at a constant value of 40 mM all along the experiment, the maximum current value was not maintained. Current decreased progressively in both reactors in a period of 20 days, reaching a final value at day 31 of $4.9 \pm 0.8 \text{ A m}^{-2}$.

Stage IV: Stabilization – long term current phase: Starting from day 31 of the experiment, the decrease in the electrocatalytic activity of the biofilm changed its slope, to a less drastic one, reaching an average current density value of $3.7 \pm 0.1 \text{ A m}^{-2}$ at day 55. The loss of current density in comparison to J_{max} reached at stage II was of $62.5 \pm 0.8\%$. This not only corroborated the same behavior between duplicates, but also a loss of the electrochemical activity of the bioanodes of more than 60% of their maximum capacities.

Epifluorescence microscopy images performed at day 55 showed a complete coverage of the Stainless Steel (SS) microelectrode by the salt marsh EAB. The scanning electron microscopy (SEM) image confirmed this since the biofilm exhibited a dense and compact rearrangement of cells, tightly spaced within each other.

As the results presented were reproducible in terms of current production curves, the experimental conditions were repeated in the sections below. Figure S2 shows the totality of the normalized current density curves obtained for this work (16 curves) with the removal of the lag phase. Despite the duration of the lag-phase (stage I), the kinetic behavior was reproducible for stage II. This trend was followed by a decrease in current in all cases (stage III and IV). Thus, the first conclusion indicates that microelectrodes are a very convenient tool to study the mechanisms of biofilm formation since they are able to successfully reproduce the same behavior in terms of catalytic activity of the bioanode as for large-scaled electrodes.

Spatiotemporal investigation of biofilm thickness and cell viability

The experiment described in the previous section was repeated four times in duplicates. However, in this case, the experience was stopped at four strategic points, corresponding to the end of the four stages previously described. The experiments were one more time conducted in duplicates, as seen in Figure 2. A cyclic voltammetry (CV) was also performed. As soon as the experiments were stopped, the biocolonisation including differentiation between cells and biopolymers and between living and dead cells was imaged with SEM and confocal laser scanning microscopy (CLSM) as seen in Figure 3. Note that for SEM, biofilms or cell aggregates are chemically dehydrated on the microelectrode surface. Cracks in the biofilm structure are sometimes visible in the SEM images for this reason. At each stage, biofilm thickness, biofilm growth rate and cell viability were primarily quantified using numerical methods associated

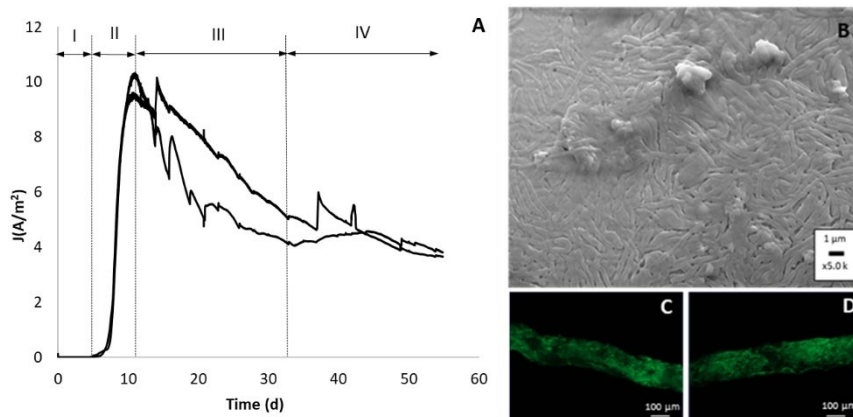


Figure 1. (A) Current production versus time for duplicate experiments obtained with stainless steel microelectrodes colonized by salt marsh EABs under constant potential of 0.1 V/SCE. (B) Scanning electron microscopy imaging of the biofilm surface over the stainless steel microelectrode. (C, D) Biofilm imaging by epifluorescence microscopy after staining the electrode with acridine orange.

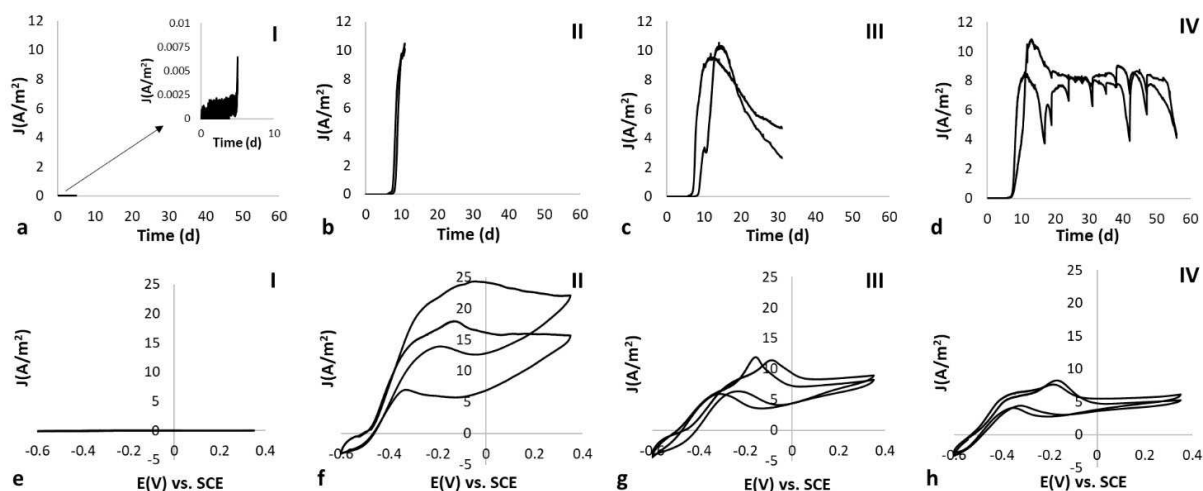


Figure 2. Evolution of current density versus time for duplicate experiments (a–d) at different stages of the experiment and their corresponding final cyclic voltammetry at a scan rate of 1 mV s^{-1} (e–h), (I) at $t = 5$ days, (II) at $t = 11$ days, (III) at $t = 31$ days and (IV) at $t = 55$ days of experiment.

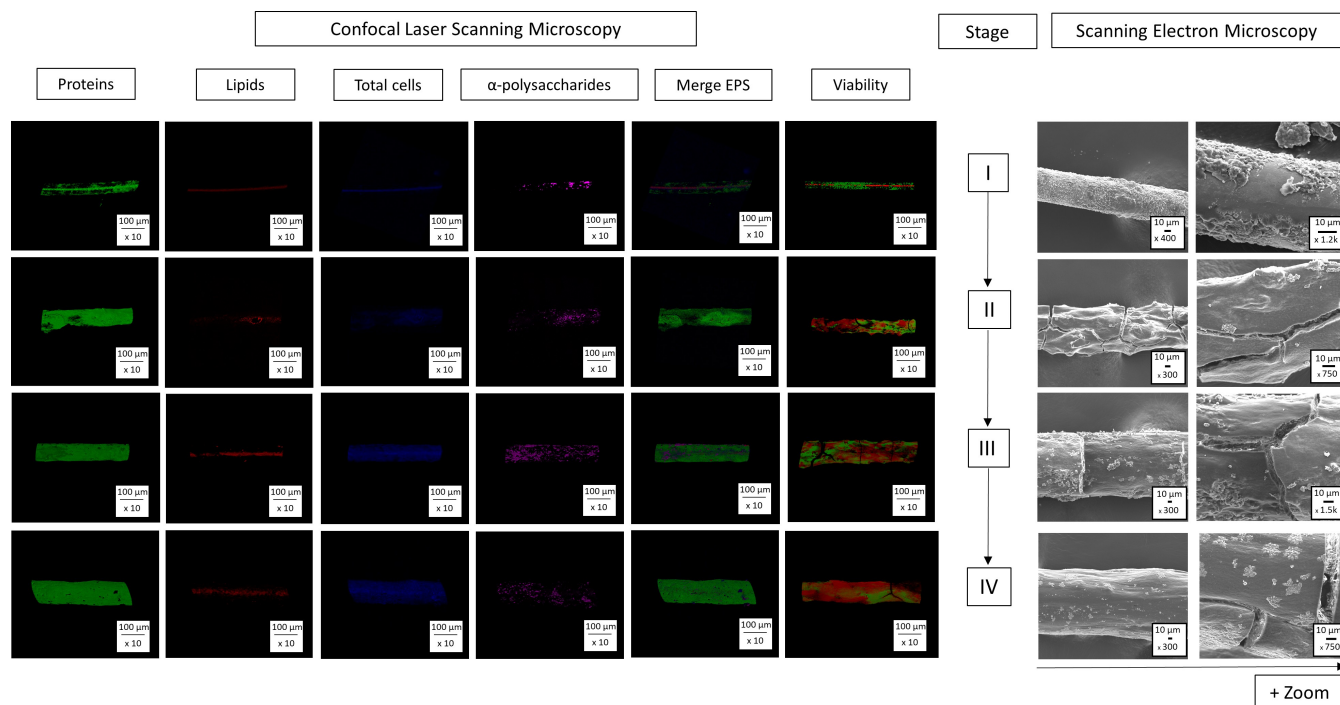


Figure 3. CLSM 3D-images and SEM images of salt marsh biofilms formed on stainless steel microelectrodes at each of the four stages.

with image analysis. Results are summarized in Figure 4, and more detailed information can be found in Table S2.

At stage I, the average thickness of biofilms was of $6.2 \pm 1.1 \mu\text{m}$ and the colonization of the biofilm over the microelectrode was heterogeneous, where different cell clusters were observed in the electrode surface. Average current measured in this point was of $0.005 \pm 0.001 \text{ A m}^{-2}$. The counting of dead cells was the minimum for this stage, where CLSM viability images showed the microelectrode surrounded mostly by living cells.

At stage II, six days later, the biofilm reached a thickness of $32.1 \pm 5.7 \mu\text{m}$, with a maximum biofilm growth rate of $4.3 \mu\text{m}$ per day. At this point, current density was at its maximum of

$10.2 \pm 0.4 \text{ A m}^{-2}$. The SS microelectrode appeared now to be completely colonized by the biofilm. The average percentage of dead cells increased to $65.2 \pm 6.3\%$ in the outer layer of the biofilm. The rapid growth of the biofilm, while reaching the limit of its electrochemical activity, may have also contributed to the accumulation of inactive cells.

At stage III, current dropped to an average value of $3.7 \pm 1.4 \text{ A m}^{-2}$. The thickness of the biofilm kept on increasing but with a lower rate of $0.8 \mu\text{m}$ per day. The structure of the biofilm was less rough and appeared to be more compact, as seen in scanning electron microscopy images in Figure 3.

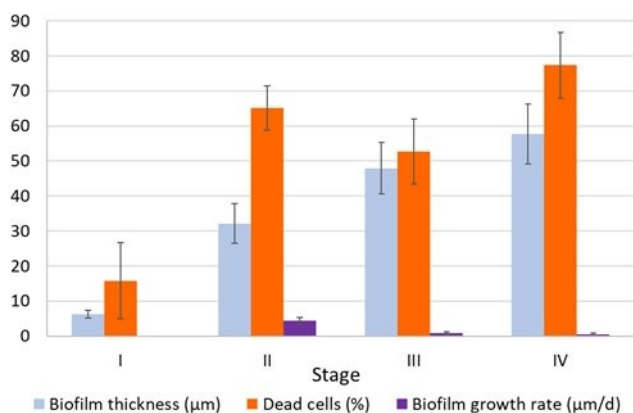


Figure 4. Evolution of the biofilm thickness, the biofilm growth rate and the percentage of dead cells in each of the four stages.

Finally, for the reactors stopped at stage IV, average registered current density was of $4.2 \pm 0.1 \text{ A m}^{-2}$. At this stage, current density values should have been lower than in stage III; however, salt marsh EABs still performed better in the reactors intended for stage IV. Biofilm growth rate was only $0.4 \text{ } \mu\text{m}$ per day, with no significant changes in the structure of the biofilm comparing with stage III. The percentage of dead cells reached the maximum value of $77.3 \pm 9.3\%$.

In addition, cyclic voltammograms from different stages showed a progressive evolution on the anodic catalytic properties of the biofilm (Figure S3 for more detail). At stage I, the electrode was barely colonized; therefore, the anodic current was low independently of the potential. A reversible redox system centered around -0.1 or -0.2 V/SCE can be seen in Figure S3 (I). At stage II, when the maximum current production was measured, a catalytic signal [Figure 2 (II)] was observed from about -0.5 V/SCE and the plateau of the maximum catalytic current was reached from -0.3 V/SCE . At the plateau, a large hysteresis was observed between the forward scan and the return scan of the voltammetry. This hysteresis would result from a capacitive effect of the biofilm and the electrode, to which would be added the reversible redox system already detected at the end of stage I. Starting from stage III, the capacitive current seemed to diminish. Theoretically, the higher the charge accumulation in the biofilm or at the electrode-electrolyte interface, the greater the capacitive effect results in a large hysteresis between the forward and return scan on the voltammogram. At stages III and IV, when current was lower, the shapes of the CVs were similar. The reversible redox system centered around -0.1 or -0.2 V/SCE is still present. This suggests here that there are at least two combined redox systems, one operating under turn-over conditions and providing electrocatalytic oxidation of acetate substrate from -0.5 V/SCE , and the other providing reversible electron transfer but around a different potential centered around -0.1 or -0.2 V/SCE . Further analysis of these two redox systems from voltammograms obtained under non-catalytic conditions (substrate depletion condition) might have identified whether these

systems are already known^[31,32] and whether they are intimately connected.^[33]

The changes on biofilm viability showed an external layer evolving from active cells at the start of the experiment towards a dead cell outer-layer by the end. Despite precautions, the possibility that the exposure to oxygen may have inactivated certain external cells when removing the bioanode from the reactors for dye labeling did not seem to be an influencing factor since the biofilm with the smallest biovolume had the higher amount of viable cells. Although it was not possible to quantify the ratio of live/dead cells in the inner layers of the biofilm (probably only for stage I where the biofilm was still very thin) since the cylindrical geometry of the bioanode only allowed the quantification in the outer layer, the trend seemed to match previous observations for EABs applying the same dead/live staining protocol. In these cases, an inner active core is surrounded by inactive cells, where it would appear that current production was achieved by the cells near the electrode surface. However, when the biofilm reaches a specific thickness threshold, the cells farther away from the electrode become limited in terms of respiration rates. The distant solid electron acceptor makes these cells unable to contribute to biofilm growth and sustained current production.^[13,34,35] The opposite case, an inner dead core and an external viable layer was also reported. In these cases, biofilm internal acidification due to acetate oxidation and diffusional gradients inside the biofilm, as well as the fraction of reduced and oxidized extracellular components involved in the electric conductivity such as c-type cytochromes, could lead to an internal layer of dead cells.^[10,19] In this case, it was proved that the outer layer was responsible for current production whether the inner dead-layer served as a conductive matrix.^[16,36]

Our results affirm that the biofilm must be growing and their cells must be active to express electroactivity. Therefore, although thick biofilms up to $57.7 \pm 8.5 \text{ } \mu\text{m}$ can be formed, the maximum electrochemical activity was found at a much thinner thickness of $32.1 \pm 5.7 \text{ } \mu\text{m}$. SEM images showed that the major growth in biovolume occurred between stage I and II, matching with the increasing current density slope in the chronoamperometry. From the end of stage II, electroactivity dropped and the viability of the anode kept on decreasing together with the biofilm growth rate. Starting from stage III onwards, it would appear that the biofilm underwent very slight changes. In terms of morphology, SEM images showed very similar structures between stage III and IV. Current reached a steady state and the amount of dead cells in the external surface augmented. Biovolume increased but at the lowest pace. At these final stages, the thickening of the biofilm was possibly related to higher exopolymeric substances secretion rather than cell multiplication.

Spatiotemporal investigation of exopolymeric substances, microbial populations and soluble electron acceptors

A new series of experiments (four experiences) was launched with the objective of continuing the study at the four stages

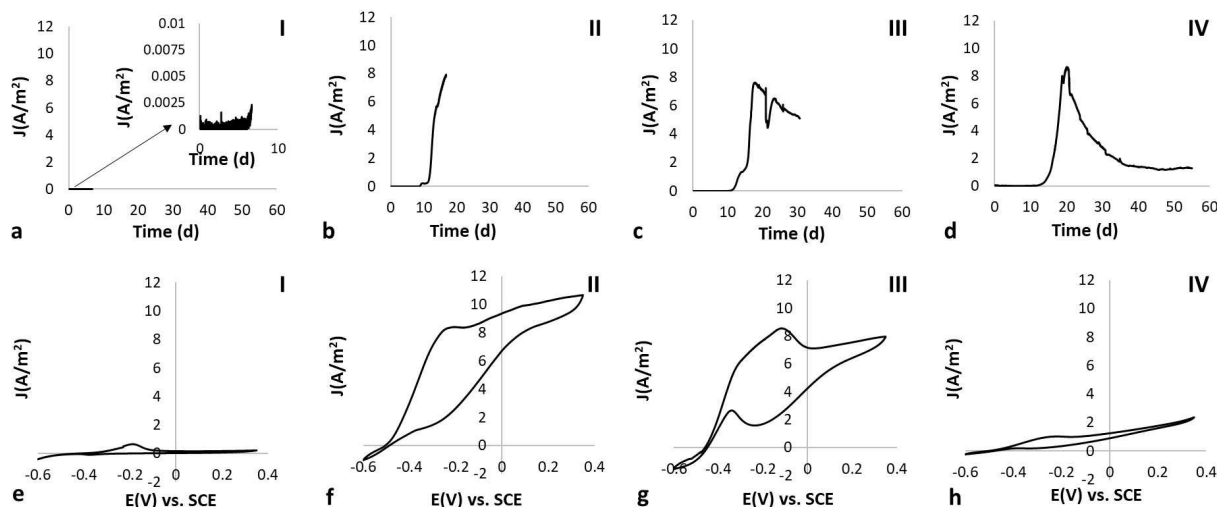


Figure 5. Evolution of current density versus time for duplicate experiments (a–d) at different stages of the experiment and their corresponding final cyclic voltammetry at a scan rate of 1 mV s^{-1} (e–h), (I) at $t = 7$ days, (II) at $t = 11$ days, (III) at $t = 31$ days and (IV) at $t = 55$ days of experiment.

(Figure 5), focusing on the evolution EPS composition and the dynamics of microbial population. The 3D representations of the biovolumes from different EPS (proteins, lipids, α -polysaccharides and total cells) obtained from the CLSM analysis are

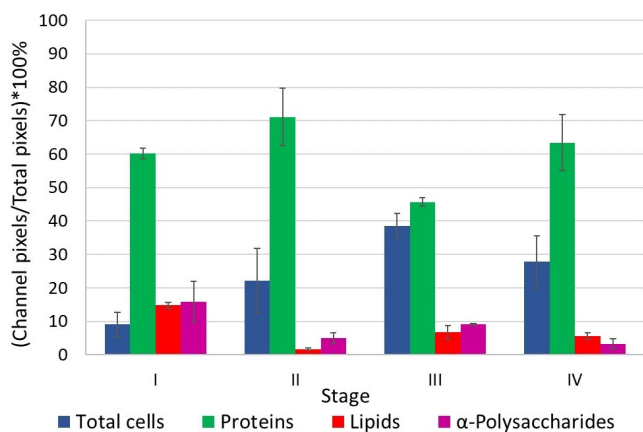


Figure 6. Bar chart illustrating the evolution of EPS composition at each of the four stages.

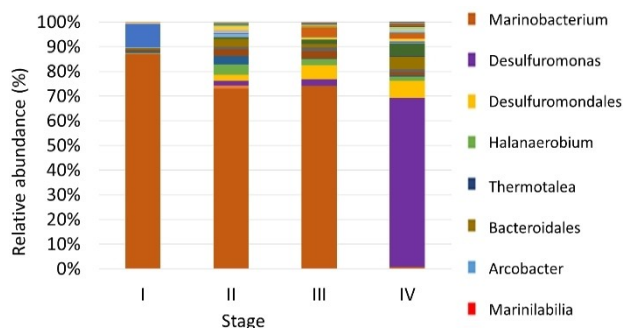


Figure 7. Relative abundance of different order or genera at the four stages of biofilm formation. Main abundances are resumed in the list on the right.

presented in Figure 3. Following the post-processing of CLSM images, the quantification of the EPS percentages at each stage are graphically represented in Figure 6 and centralized in Table S2.

The results of the relative abundances of the different bacterial orders and genera present in the biofilms at the four stages of bioanode formation are summarized in Figure 7 and Table 1. The analysis goes until the genera level in all cases with the exception of *Desulfuromonadales* and *Bacteroidales*, which correspond to the order level. It is worth clarifying that *Marinilabilia* classifies into the *Bacteroidales* order and *Desulfuromonas* to *Desulfuromonadales*. In addition, Table S3 shows the results of inductively coupled plasma (ICP) analysis of the evolution in the concentration of sulfur, iron and manganese contained in the synthetic medium.

At stage I, current density did not exceed a value of 0.002 A m^{-2} . For the determination of the components of the polymeric matrix at this stage, the biofilm was mainly composed by proteins at a percentage of $60.2 \pm 1.6\%$. In terms of bacterial diversity, there was an important dominance of *Marinobacterium* with 87.0% of abundance. This was followed by *Arcobacter* with 9.3% .

Table 1. Detailed relative abundance at different order or genera in the biofilm at the end of each stage. The three more relevant microbial abundances for each stage are in bold.

Order/Genera	Stage			
	I	II	III	IV
<i>Marinobacterium</i>	87.0	72.9	74.1	0.6
<i>Desulfuromonadales</i>	–	2.2	5.7	6.9
<i>Desulfuromonas</i>	–	2.0	2.6	68.5
<i>Arcobacter</i>	9.3	0.5	–	0.5
<i>Halanaerobium</i>	–	4.0	2.4	1.1
<i>Marinilabilia</i>	–	–	3.7	2.1
<i>Bacteroidales</i>	0.5	3.1	1.6	5.2
<i>Thermotalea</i>	0.7	3.5	0.2	0.5

At stage II, when current density production reached a value of 7.9 A m^{-2} , the amount of total cells increased as well as the amount of proteins. At this stage, the occurrence of proteins reached a maximum of $71.1 \pm 8.6\%$. The abundance of *Marinobacterium* decreased to 72.9% and *Arcobacter* was only scarcely present. The biofilm community became more diverse, with the appearance of other bacterial genera such as *Halanaerobium* and *Thermotalea* present at 4.0% and 3.5% respectively.

At day 31, current reached a final value of 5.1 A m^{-2} . At stage III, the biovolume of total cells over the total biovolume was the highest of the stages, reaching a value of $38.5 \pm 3.7\%$. Concerning EPS, the production in protein based polymers decreased in comparison to stage II to $45.7 \pm 1.2\%$, whereas the amount of polysaccharides almost doubled its value (from $5.0 \pm 1.5\%$ to $9.1 \pm 0.3\%$). The presence of *Marinobacterium* remained almost stable in comparison to stage II. There was an emergence of *Desulfuromonadales* order and *Marinilabilia* genera. In addition, the concentration of sulfur in the synthetic medium decreased abruptly, from 17.8 mg L^{-1} in stage II to 1.1 mg L^{-1} in stage III.

At stage IV, final current density was of 1.3 A m^{-2} . The biovolume of total cells decreased with respect to stage III, whether the production of protein polymers increased and the value for polysaccharides–protein ratio was the lowest of the series. An important shift on the genera present in the biofilm community was observed, since *Desulfuromonas* became dominant with 68.5% of abundance and the presence of *Marinobacterium* was hardly detectable.

The cyclic voltammograms showed the same trend that in the previous section. There was likewise an evolution on the biofilm, with more marked hysteresis at higher current (Figure S4 for more detail). Yet, an oxidation peak was found around -0.2 V/SCE .

The temporal evolution of the exopolymeric substances showed an increase throughout the four stages, as highlighted in the CLSM images of Figure 3, where a widening of the EPS was observed from stage I to IV. To support results from the previous section, as the biovolume of total cells diminished from stage III to stage IV, the increase of thickness between these two stages was probably due to an enlargement of the matrix rather than cell multiplication. It can be hypothesized that the presence of a thick layer of EPS could play a role as a diffusive barrier, thus preventing the substrate and/or nutrient diffusion needed for cell growth.^[37]

The EPS of electroactive biofilms work as a tridimensional conductive matrix when electrons are transferred from the bulk to the anode within the biofilm. Extracellular proteins store redox compounds, such as cytochrome-c, involved in electron transfer.^[38,39] Polysaccharides, on the other hand, are known to be in the conductive range between semiconductors and insulators, probably decreasing the electrical conductivity of the matrix.^[40] However, their presence in the matrix is essential for cell anchoring and protection mechanisms, in addition to many other structural, ion exchange and nutrient source (e.g., carbon source) functions.^[41] The highest percentage of extracellular proteins was found in stage II, in coincidence with the peak of

electrochemical activity of the biofilm. Significant positive correlation has already been found between steady-state current in mixed-culture bioanodes and protein content in EPS.^[24] For α -polysaccharides, the highest content was in stage I. Nevertheless, it is relevant not to lose sight of the fact that the temporal analysis of the matrix implies that the volume of the exopolymeric substances also evolves in time. Probably, the elevated percentage values of stage I in comparison to the rest of the series, was due to the low colonization of the electrode, which exacerbated the results. This was also confirmed with the results of CLSM images, which showed the highest polysaccharides content at stage III.

The ratio of α -polysaccharides to proteins can be seen as a useful parameter to normalize the results when analyzing the EPS evolution of EABs. The highest value was obtained at stage I, probably due to the adhesive function of polysaccharides to the anode at the early stages of biofilm formation.^[42] Later, in stage II, the ratio decreased to a third of its value and later re-increased 2.5 times at stage III. Extracellular polysaccharides production after the current peak might have decreased the conductivity of the biofilm matrix. This was already reported for *Geobacter* biofilms, where the secretion of extracellular polysaccharides was more elevated in the bioanodes with the weakest electrochemical performance.^[23] The ratio decreased for a second time at stage IV. As the percentage of total cells was lower in stage IV than in stage III, proteins content raised in the total biovolume regarding stage III, therefore decreasing the ratio of α -polysaccharides to proteins.

The dynamics of microbial community showed a sparse colonized bioanode at the end of stage I highly dominated by *Gammaproteobacteria*, mainly enriched with *Marinobacterium*. Species present in this genus were typically found in electroactive biofilms formed from natural marine environments,^[43] salt marsh sediments^[44] and hypersaline coastal lagoons.^[45] *Marinobacterium* strains are gram-negative, facultative anaerobic and they require NaCl for growth in a concentration range of 1.0 – 7.5% NaCl.^[46] *Arcobacter* species were also present in the biofilm community of the bioanode. Their abundance in coastal environments and their electroactivity were also reported.^[47–49] Their incidence at the early stages could be related to their ability of enhancing the secretion of flagellin proteins at anaerobic conditions.^[50]

At stage II, the relative abundance of the community shifted and the amount of *Marinobacterium* decreased from 87.0% to 72.9% . In addition, *Arcobacter* was merely present in the biofilm. At this step, the bacterial diversity included species from Clostridia, such as *Thermotalea* (3.5%) and *Halanaerobium* (4.0%), and from *Deltaproteobacteria* with the presence of *Desulfuromonadales* (2.2%) order and *Desulfuromonas* (2.0%). The appearance of strictly anaerobic microorganisms in the biofilm was not surprising. *Halanaerobium* is known as a halophilic electroactive bacteria,^[51] which probably grew in the highly saline environment of the synthetic medium at the early stages and then was able to colonize the electrode. At day 31, the dominance of *Marinobacterium* (74.1%) remained constant with respect to the previous stage. *Halanaerobium* abundance decreased to 2.4% and *Thermotalea* was not detectable.

Desulfuromonas increased to 2.6% and *Desulfuromonadales* order to 5.7%. In this stage, there was the appearance of *Marinilabilia* (3.7%), a facultative anaerobic bacteria usually found in mud marine sediments.

The most relevant observation from the microbial analysis occurred at stage IV. At day 55 there was a dominance of *Desulfuromonas* (68.5%) with the quasi-undetectable amount of *Marinobacterium* (0.6%). *Desulfuromonas* species were already identified in EABs from the same inoculum source.^[52] The interest in analyzing the temporal evolution in the amount of sulfur, iron and manganese in the culture medium containing the inoculum was based in the properties of certain bacteria to use these compounds as terminal electron acceptors.^[6,53] In the case of *Desulfuromonas*, species from the genera can reduce elemental sulfur to sulfide and also grow by transferring electrons to insoluble iron oxides.^[54,55] The evolution of the microbial population over time is hypothetically based on the initial planktonic growth of *Desulfuromonas* in the liquid phase through acetate oxidation and elemental sulfur reduction to sulfide. The incidence of *Desulfuromonas* in the biofilm was visible from stage II and later slightly increased in stage III, where sulfur concentration in the liquid phase decreased abruptly. As in stage III the sulfur content was scarce, probably the amount of *Desulfuromonas* present in the liquid environment had to shift their respiring mechanism from sulfur to the electrode, which could explain the prevalence of *Desulfuromonas* in the biofilm at stage IV.

It can be supposed that at the early stages *Marinobacterium* was the most efficient anode respiring bacteria, taking advantage of a fresh synthetic medium with NaCl and acetate, and prevailing in a non-strictly anaerobic environment. The temporal medium evolution along with the growth of other planktonic electroactive bacterial species that later colonized the anode led to a sharp increase in the electroactivity. Given the fact that the almost complete shift from *Marinobacterium* to *Desulfuromonas* between stage III and IV did not generate drastic changes in the catalytic activity of the bioanode and that *Marinobacterium* was present since stage I, it could be thought that it is the contribution of the minority bacteria that played the most important role in the production of current.

Late stages of biofilm formation: reversibility or irreversibility of the electrochemical activity?

A series of two duplicates were again carried out under constant polarization of 0.1 V/SCE in order to test whether at the end of stage III, the anodic current density could be reestablished to its maximum value, as seen in Figure 8. For this reason, at day 27, corresponding in practice here at the end of stage III, the polarization was stopped and a fresh batch of medium with 40 mM of acetate was added to the reactors. As no considerable change in current production was observed, the reactors were re-inoculated with salt marsh sediments on day 29. At day 55, the polarization was stopped and micro-electrodes were retrieved for future microbial population analysis.

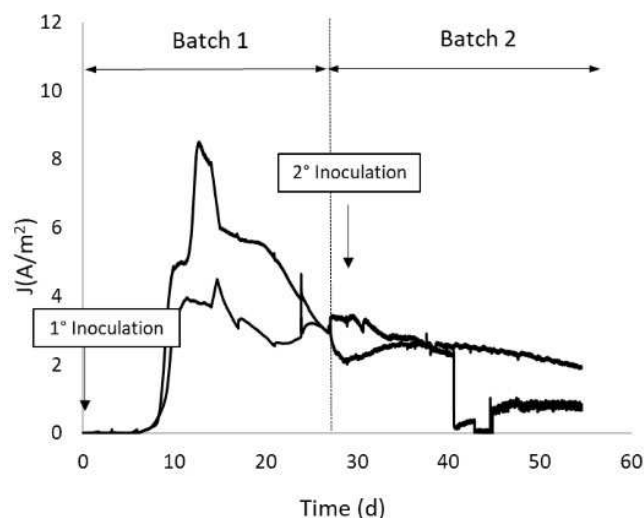


Figure 8. Evolution of current density versus time for duplicate experiments. The reactors were inoculated with salt marsh at $t = 0$ days (1st Inoculation). At $t = 27$ days, the medium was replaced with a fresh batch of Starkey medium (Batch 2). At $t = 29$ days, 30 mL of salt marsh were added to the reactors (2nd inoculation).

The average current registered before the addition was of $2.8 \pm 0.9 \text{ A m}^{-2}$ and of $2.7 \pm 0.8 \text{ A m}^{-2}$ after the inoculation. The dramatic drop of current for one duplicate at day 40 was probably due to a connection issue, since current slightly increased when the connections and the reference electrode were changed. Acetate concentration was also checked to ensure that the drop was not due to a depletion in the quantity of the electron donor. Therefore, the replacement of a new batch of medium, and consequently of inoculum, did not improve significantly the catalytic activity of the biofilm. The shape of current production profiles showed the same trend that in the sections above.

The results discard the hypothesis that working in batch mode can lead to the depletion of certain bacterial nutrients or components in the medium, which could work as electron shuttles. Strategies linked to medium replacement were already described for *S. Oneidensis* biofilms to probe mediated electron transfer^[56] and also for *G. Sulfurreducens* to demonstrate that the cells attached to the anode surface were responsible for current production.^[57] In the case that bacteria could use soluble compounds for electron transfer, current would have increased considerably when replacing the medium. Examples of in current production were already observed when switching from real medium BES operation to synthetic medium. This was due to the resupply in vitamins or minerals present in the synthetic medium and/or the absence of dissolved electron acceptors, such as nitrates and sulfates, that could compete with the electrode to accept electrons.^[14] Working with a synthetic medium from the start of the experiment avoids the presence of electron sinks, which proved to be the case as the electrochemical activity of the biofilm was not improved. This is also consistent with what was observed for the cyclic voltammeteries in Figure S5. The difference between Batch 1 and Batch 2 could be due to the biofilm short exposure to air when replacing the

medium. In addition, before and after inoculation, curves were also similar.

Relative abundance of microbial population at day 55 showed two biofilms with the same dominance but in different proportions. *Marinobacterium* accounted to 38.3% and *Desulfuromonas* to 44.3% in the sample with the highest current peak. In the other replicate, *Marinobacterium* only represented 9.8%, while *Desulfuromonas* constituted 14.1% and *Desulfuromonadales* 33.0%. Therefore, the total presence of sulfur reducing bacteria was similar in both cases, yet minor than in the bioanode at stage IV in the previous section (68.5%). This means that what the change of medium might have affected is the amount of sulfur-reducing bacteria already grown in the liquid electrolyte at day 27. In the previous section, it was described that the period between stage II and III corresponded to the depletion of sulfur in the liquid environment. Re-inoculation on day 29 probably restored sulfur concentration, giving the possibility to sulfur-reducing bacteria to proliferate, grow and later colonize the electrode.

General discussion

Microbial bioanodes formed on stainless steel microelectrodes with salt marsh inoculum at an applied potential of 0.1 V/SCE accurately reproduced the classical time evolution of the electrochemical activity of biofilms already reported with macro-scale bioelectrodes. The long-term (> 50 days) loss of J performance was also consistent with that described in the literature, ranging from 30 to 50% of J_{\max} . This systemic study on mixed population electroactive biofilms, including microscopic, electrochemical, biochemical and microbiological characterisations, allowed significant progress to be made on the correlation between anode current production and the spatio-temporal evolution of mixed population microbial biofilms on metallic anodes.

In terms of biocolonisation on the surface of the stainless steel microelectrode, the bacterial cells initially developed as isolated clusters until they gradually formed a thick homogeneous layer on the surface of the microelectrode. This rough-edged structure then became much smoother at the end of stage III, mainly due to the production of EPS. Regarding the kinetics of biofilm growth and thickening, the biofilm reached maximum electrochemical activity at a thickness of $\approx 32 \mu\text{m}$ while growing at a rapid rate ($4.3 \mu\text{m/d}$). However, the electrochemical activity then decreased, accompanied by a lower growth rate ($0.4 \mu\text{m/d}$) which led to an increasing thickness to $\approx 57 \mu\text{m}$. The cell viability rate also changed significantly as the biofilm thickened for 17 days. The high viability in the early stages of biocolonisation suggested that current generation was more related to viability rate than to biofilm thickness.

The role of the biofilm EPS matrix and its evolution over time in relation to the electrochemical activity of the biofilm is not yet so simple to explain. On the one hand, when the microbial biofilm reaches a threshold thickness, electron transfer can be quite limited depending on the mechanisms used by the exo-electrogenic microorganisms. Mixed population bioan-

odes add further complexity because several types of electron transfer mechanisms coexist and because insulating, non-active EPS, hindering the chemical diffusion of species, can be synthesized by non-electroactive microbial populations. On the other hand, the progressive production of EPS, and the change over time of the chemical composition of the EPS matrix also has an impact on the overall electrical conductivity of the biofilm. In the early stages of biocolonisation, as soon as the biofilm adhered to the anode, the ratio of polysaccharides to proteins was balanced in favour of the protein content, meaning that the electrical conductivity of the matrix was increased. In addition, the coupled effect of a thin and more viable biofilm probably annihilated all kinds of gradients as well as promoting metabolic and electrochemical processes accordingly. After the current reached its peak J_{\max} , the widening of the EPS matrix and the specific accumulation of polysaccharides, at the detriment of proteins, inhibited the possibility of maintaining a stable and high current approaching the maximum value.

The temporal distribution of microbial populations showed that the time of biocolonisation associated with the continuous production of anodic current progressively affected the bacterial community of biofilms established on the surface of stainless steel microelectrodes. The radical shift from a strong predominance of *Marinobacterium* during stages I and II to *Desulfuromonas* especially during stage IV was explained by the depletion of sulphur in the liquid medium and the growth of sulphate-reducing bacteria that subsequently colonized the electrode.

Since *Desulfuromonas* is known to be electroactive, this respiring-anode bacterial rearrangement alone could not explain the sharp loss in the electrochemical activity that is observed. Apart from the fact that electrochemical activity based on much slower electron transfer mechanisms than those engaged by *Marinobacterium* would be a plausible explanation. However, it is still open for discussion whether subtle changes in microbial abundance from one stage to the next play an important role in the performance of the bioanode or not.

The regeneration of the synthetic liquid medium when the biofilm has reached stage III of development did not seem to have any impact on the electrochemical activity of the biofilm. It would therefore indicate that after the current peak and its consequent drop, the loss of electrochemical activity is irreversible. Re-inoculation with fresh salt marsh sediment also confirmed the evolution of the microbial population in the bioanode by obtaining a dominant relative abundance of sulphur-reducing bacteria in the last stage of biofilm formation.

Finally, the use of microelectrodes for the study of electroactive biofilms opens up attractive research prospects since it offers more homogeneous and less limited study conditions in terms of electrode potential distribution, mass transfer and biocolonisation.^[28] Their small size allows for freedom from risky post-experimental slicing and other manipulations that could affect the integrity of the biofilms prior to their microscopic analysis. Also analytical post-processing such as fixation, dehydration or staining and labelling are more homogeneous as the chemical diffusion fronts progress without major limitations. Microelectrodes also offer the possibility of integra-

tion into transparent microdevices. By downscaling the liquid bulk-biofilm-anode interface, in-situ and real-time non-invasive investigation of local phenomena could give more hints of the spatiotemporal evolution of microbial anodes and its link to the loss of electroactivity. These technologies can contribute to a deeper understanding of gradients inside the biofilm, bacterial adhesion and biofilm formation, the effects of hydrodynamics and of the liquid electrolyte, among others. In addition, efforts should also be made to implement a more accurate viability detection method than the one routinely used nowadays. To gain more knowledge about how proteins and polysaccharides are formed in the matrix, and how to optimize their production could be an interesting scope of study in terms of bioanode conductivity.

Conclusion

The distinctive electrochemical behaviour of multi-species bioanodes was successfully reproduced in micro-sized electrodes, where four distinct temporal stages of biocolonisation and electrochemical activity were extensively described. To the best of our knowledge, this is the first time investigation of biofilm electrochemical activity, spatial bacterial cells viability, EPS production and composition, and relative abundance of microbial biofilm population has been performed simultaneously with a spatiotemporal approach. From the early stages of biocolonisation of the stainless-steel microelectrode to the peak of current production J_{\max} , the maximum growth rate of the biofilm, the high viability and the high content of extracellular proteins in the matrix, favored the auspicious electrochemical activity. After the maximum J_{\max} peak was reached, the loss of electrochemical performance turned irreversible. This was coupled with a decrease in biofilm growth rate, an accumulation of dead cells and an increase in the proportion of polysaccharides in the EPS matrix. In addition to a chemical evolution of the biofilm, the shift of the microbial community from *Marinobacterium* to *Desulfuromonas* also reflects a microbial evolution of the biofilm. Focusing on the early stages of biofilm development and understanding how to control the phenomena that promote current production until it reaches its maximum, and how to avoid the processes that subsequently adversely affect electrochemical activity, should be a research priority to improve the long-term functioning of multi-species microbial bioanodes.

Experimental Section

Inoculum origin and synthetic medium

Sediments collected from a salt marsh (Mediterranean Sea coast, Gruissan, France) were used as microbial inoculum. The sediments were stored in a sealed recipient at room temperature until use. A volume of 30 mL of sediments was mixed with 600 mL of synthetic medium based on the Starkey medium (NH_4Cl 2.0 g L⁻¹, K_2HPO_4 0.5 g L⁻¹, NaCH_3COO 40 mM, HCl 37% 46 mL, $\text{MgCl}_2 \cdot 6\text{H}_2\text{O}$ 55.0 mg L⁻¹, $\text{FeSO}_4(\text{NH}_4)_2\text{SO}_4 \cdot 6\text{H}_2\text{O}$ 7.0 mg L⁻¹, $\text{ZnCl}_2 \cdot 2\text{H}_2\text{O}$

1.0 mg L⁻¹, $\text{MnCl}_2 \cdot 4\text{H}_2\text{O}$ 1.2 mg L⁻¹, $\text{CuSO}_4 \cdot 5\text{H}_2\text{O}$ 0.4 mg L⁻¹, $\text{CoSO}_4 \cdot 7\text{H}_2\text{O}$ 1.3 mg L⁻¹, BO_3H_3 0.1 mg L⁻¹, $\text{Mo}_2\text{O}_7(\text{NH}_4)_6 \cdot 4\text{H}_2\text{O}$ 1.0 mg L⁻¹, $\text{NiCl}_2 \cdot 6\text{H}_2\text{O}$ 0.05 mg L⁻¹, $\text{Na}_2\text{SeO}_3 \cdot 5\text{H}_2\text{O}$ 0.01 mg L⁻¹, $\text{CaCl}_2 \cdot 2\text{H}_2\text{O}$ 60.0 mg L⁻¹) with the addition of 45 g L⁻¹ of NaCl.

Reactor design, microelectrode fabrication and electrochemical techniques

Each reactor (Duran Schott type glass 550 mL) was equipped with a three-electrode system (Figure S1). A twist-off lid with four circular openings was set at the top of the reactor allowing the insertion into the medium of the three electrodes. Stainless steel microelectrodes were implemented as working electrodes. For its design, 15 cm of copper wire was welded into a 2 cm wire of stainless steel ($\varnothing = 50 \mu\text{m}$, Goodfellow). The system was threaded into a plastic tip and sealed with an inert resin (Epofix). The upper end was welded to a connector that served as electrical connection, while the bottom end served as the working electrode. Platinum grids previously cleaned under the flame were used as counter electrodes. A saturated calomel electrode with a fixed potential of +0.248 V/SHE (SCE, Radiometer Analytical) was set between the counter and working electrodes. A fourth remaining opening was used for sampling addition. The medium was purged with nitrogen for 20 minutes to eliminate oxygen before launching the electrochemical techniques. The working electrode potential was controlled under the operation of a multichannel potentiostat (Biologic SA) operated by a data acquisition software that permits the control of the potentiostat (Ec-Lab). Stainless steel microelectrodes were constantly polarized at 0.1 V/SCE. 40 mM of sodium acetate was used as a substrate. COD (Chemical Oxygen Demand) levels were regularly monitored and kept at a value of 2560 mg O₂ L⁻¹ to correspond to the equivalent of 40 mM of sodium acetate. LCK 514 COD kits (Hach Lange, range of measurement 100–2000 mg O₂ L⁻¹) were used for COD measurements. Samples for the COD measurement were previously filtered with a chloride filter kit Hach LCW925 (Hach Lange). When the polarization was stopped, cyclic voltammetry at 1 mV s⁻¹ was performed in the range of potential from -0.6 V/SCE to 0.35 V/SCE. Three successive cycles were performed, the second scan was only presented.

Microscopy

Staining of EABs

For the imaging of total cells, samples were labeled with a solution of acridine orange at 0.01% (A6014, Sigma) for approximately 20 minutes and then carefully rinsed with physiological solution (NaCl 0.9 g L⁻¹).

The exopolymeric matrix of the biofilm was marked by using a mix of four fluorescent dyes: Concanavalin A tetramethylrhodamine conjugate (ConA-TMR, Thermofischer Scientific) for α -polysaccharides, fluorescein isothiocyanate isomer I (FITC, Merck) for proteins, 1,1'-dioctadecyl-3,3',3'-tetramethylindocarbocyanine perchlorate (DiD oil, Merck) for lipids and 4',6-diamidino-2-phenylindole dihydrochloride (DAPI, Merck) for total cells. 25 mL of working solution was prepared in physiological solution with the following concentrations: FITC at 0.05 g L⁻¹, DAPI at 1.05×10^{-4} g L⁻¹, Con-A TMR at 0.1 g L⁻¹ and DiD oil at 0.08 g L⁻¹. Microelectrodes were set in contact with the working solution for 30 minutes then carefully rinsed with physiological solution.

Dead/Live assessment was carried by treating the samples as soon as they were retrieved from the reactor with a mix of SYTO 9 (7.5 μM in final solution) and Propidium Iodide (PI) (0.015 g L⁻¹ in

final solution) diluted in physiological solution (Live/Dead BacLight Bacterial Viability Kits L7012, Thermofischer Scientific).

In all cases, once rinsed, the electrodes were left out in the open air and protected from the light to dry for at least 24 hours before observation.

Epifluorescence microscopy

Biofilms stained with acridine orange were imaged with a Carl Zeiss Axio Imager-M2 microscope (Carl Zeiss) equipped for epifluorescence with an HXP 200C light source and the Zeiss 09 filter (excitor HP450r HP450200 C light source). Biofilms were observed with the objective EC Plan-Neofluar 10x/0.30. Images were acquired with a digital camera (Zeiss AxioCam MRm) along the Z-axis and the set of images was processed with the Zen (Carl Zeiss) software. For each sample, two observations were made. The Zen (Carl Zeiss) software optimized the z-step of the stack. Thickness was measured with the toolbox of the Zen (Carl Zeiss) software, taking nine points per image. Biofilm growth rate was calculated as the increase of thickness divided by the time interval.

Biofilm thickness was calculated as the diameter of the colonized microelectrode ($\varnothing_{\text{total}}$) minus the diameter of the blank microelectrode ($\varnothing_{\text{microelectrode}}$) obtained from microscopic images, as in in [Eq. (1)]. An average biofilm thickness value was calculated from 9 microscopic acquisitions.

$$\delta_{\text{Biofilm}} = \frac{\varnothing_{\text{total}} - \varnothing_{\text{microelectrode}}}{2} \quad (1)$$

Confocal laser scanning microscopy and image analysis

The exopolymeric matrix of the biofilm and biofilm viability was imaged with a Leica SP8-2017 microscope (Leica Microsystems) with the Leica Application Suite X: LAS-X software (Leica Microsystems). The image acquisition was made by using the HC PC FLUOTAR 10x/0.30 objective in dry immersion. For each sample, two stacks of horizontal plane images (1024×1024 pixels) were taken from two randomly chosen areas. The LAS-X software optimized the z-step of the stack depending on the sample. Once the acquisition was completed, the LAS-X software represented the projection of the stack in a 3D view.

For image analysis, 3D images were treated with the Image J software. In the case of viability analysis, since a two-color image was obtained, the color threshold tool was used. For the analysis of the exopolymeric substances, as the sample was treated with four different stains, the 3D images were treated individually channel by channel, corresponding to each component in the exopolymeric matrix of the biofilm. First, the color image was transformed into an 8-bit image and later a threshold value was set. The threshold value allows the labeling of each pixel as empty or marked.

After, the software showed the amount of empty pixels by image, and the calculation of marked pixels per image was calculated as the difference between total pixels and empty pixels.

For the viability analysis, eight images were treated. The amount of dead cells (cells labeled with PI) is the ratio of PI labeled pixels over the total pixels, as calculated in [Eq. (2)]:

$$\text{Dead cells [\%]} = \left(\frac{\text{PI pixels}}{\text{PI pixels} + \text{SYTO 9 pixels}} \right) \times 100\% \quad (2)$$

For the EPS analysis, four biofilms were observed in two random sections for the four different stains, resulting in a total of thirty-two images processed. The amount of each component was calculated as the ratio of the channel pixels over the total pixels. For the case of proteins, it is described in [Eq. (3)] as it follows:

$$\text{Proteins [\%]} = \left(\frac{\text{FITC pixels}}{\text{FITC pixels} + \text{DAPI pixels} + \text{DID oil pixels} + \text{ConA pixels}} \right) \times 100\% \quad (3)$$

This was likewise calculated for total cells, lipids and α -polysaccharides.

Scanning electron microscopy

The samples were metallized with gold (Au) prior to observation in order to reduce charging effects. Samples were observed under the scanning electron microscope Leo 435 VP-Carl Zeiss SMT.

Microbial population analysis

Microelectrodes containing the EABs were stored in 2 mL Eppendorf tubes. 150 μ L of PCR grade water and a spatula tip of 425–600 μ m glass beads (G8772, Sigma) were added to the tubes. A negative control was made with only water and beads. Two one-minute mechanical grindings with a robot (Fast-prep 24 MP Biomedicals, Thermofischer Scientific) at a maximum speed of 6.5 ms^{-1} were performed to loosen the biofilms formed on the surface of the microelectrode. The clean microelectrode was retrieved from the tube and the remaining suspension was subjected to two thermal shocks by alternating ice and water bath at 95 °C for 1 min each time, in order to lyse the cells and release the DNA.

The 16S amplification was then performed on 1 μ L of the suspension with the GoTaq Flexi G2 enzyme (Promega) with the primers:

Genewiz515Fmod:5'-ACACTCTTCCCTACGACGCTCTCCGATCTGT-GYCAGCMGCCGCGGTAA-3'

Genewiz806Rmod:5'-GACTGGAGTTCAGACGTGTGCTCTCCGATCTG-GACTACNVGGGTWCTAAT-3'

35 cycles of PCR were carried at a temperature of 55 °C. The primers were designed to contain overhang compatible sequences with Nextera XT index (Illumina). The purified amplicons were sequenced using the MiSeq platform (Illumina).

Microbiome bioinformatics were performed by the open-source software QIIME2, version 2021.11 (<https://qiime2.org>).^[58] Raw reads were demultiplexed, quality-filtered, denoised and chimera-checked using DADA2.^[59] DADA2 uses a parametric model to infer true biological sequences from reads. The model relies on input read abundances (true reads are likely to be more abundant) and the pairwise similarity between sequences. Sequences were aligned using MAFFT,^[60] and were used to construct a phylogeny using FastTree.^[61] The taxonomic annotation of the resulting amplicon sequence variants (ASVs) was assigned using the feature-classifier command with default parameters in QIIME2 and sequences were matched against the Greengenes 13_8 database.^[62] Finally, scaling with ranked subsampling (SRS) curves^[63] were drawn to determine whether the sequencing depth was sufficient to represent the true diversity of the samples.

Inductively coupled plasma analysis

Sulphur, iron and manganese concentration was determined from the reactors. 5 mL of the analyte were taken at the time of 7, 11, 31 and 55 days. The samples were diluted with distilled water to a volume of 20 mL and then filtered to remove chloride ions. Chloride filter kit Hach LCW925 (Hach Lange) was used for filtration. Every sample was treated with 3 mL of HNO₃ 65% for analysis. Calibration solutions for sulfur, iron and manganese were prepared by diluting a certified solution of the elements of 1000 µg mL⁻¹ in the synthetic medium. It was diluted in a 1:4 ratio and treated with 3 mL of HNO₃ 65% for analysis. The solutions were analyzed using an Inductively Coupled Plasma Optical Emission Spectroscopy (ICP-OES) SS Ultima 2 (Horiba). Sulfur quantification was measured at a wavelength of 180.676 nm, iron at 259.940 nm and manganese at 257.610 nm.

Acknowledgements

This work was part of the "MICROBE" project funded by the French "Agence Nationale de la Recherche" grant number ANR-18-CE05-0024.

Conflict of Interest

The authors declare no conflict of interest.

Data Availability Statement

The data that support the findings of this study are available from the corresponding author upon reasonable request.

Keywords: electrochemistry · extracellular polymeric substances · oxidation · salt marsh bioanodes · stainless steel microelectrodes

- [1] B. Erable, N. M. Duțeanua, M. M. Ghangrekar, C. Dumas, K. Scott, *Biofouling* **2010**, *26*, 57–71.
- [2] F. Harnisch, U. Schröder, *Chem. Soc. Rev.* **2010**, *39*, 4433–4448.
- [3] A. A. Mier, H. Olvera-Vargas, M. Mejía-López, A. Longoria, L. Vereia, P. J. Sebastian, D. M. Arias, *Chemosphere* **2021**, *283*, 131138.
- [4] S. Jung, J. Lee, Y. Park, E. E. Kwon, *Bioresour. Technol.* **2020**, *300*, 122748.
- [5] M. Rimboud, D. Pocaznoi, B. Erable, A. Bergel, *Phys. Chem. Chem. Phys.* **2014**, *16*, 16349–16366.
- [6] D. R. Bond, D. E. Holmes, L. M. Tender, D. R. Lovley, *Science* **2002**, *295*, 483–485.
- [7] C. E. Reimers, L. M. Tender, S. Fertig, W. Wang, *Environ. Sci. Technol.* **2001**, *35*, 192–195.
- [8] T. H. Pham, P. Aelterman, W. Verstraete, *Trends Biotechnol.* **2009**, *27*, 168–178.
- [9] W. H. Tan, S. Chong, H. W. Fang, K. L. Pan, M. Mohamad, J. W. Lim, T. J. Tiong, Y. J. Chan, C. M. Huang, T. C. K. Yang, *Processes* **2021**, *9*, 1–13.
- [10] D. Sun, J. Chen, H. Huang, W. Liu, Y. Ye, *Int. J. Hydrogen Energy* **2016**, *41*, 16523–16528.
- [11] R. J. Steidl, S. Lampa-Pastirk, G. Reguera, *Nat. Commun.* **2016**, *7*, 12217.
- [12] P. S. Bonanni, D. F. Bradley, G. D. Schrott, J. Pablo, *ChemSusChem* **2013**, *6*, 711–720.
- [13] G. L. Chadwick, F. J. Otero, J. A. Gralnick, D. R. Bond, V. J. Orphan, *Proc. Natl. Acad. Sci. USA* **2019**, *116*, 20716–20724.
- [14] M. Oliot, P. Chong, B. Erable, A. Bergel, *Chem. Eng. J.* **2017**, *327*, 218–227.
- [15] E. Blanchet, E. Desmond, B. Erable, A. Bridier, T. Bouchez, A. Bergel, *Bioresour. Technol.* **2015**, *185*, 106–115.
- [16] R. Renslow, J. T. Babauta, A. C. Dohnalkova, M. I. Boyanov, K. M. Kemmer, P. D. Majors, J. K. Fredrickson, H. Beyenal, *Bone* **2013**, *23*, 1–7.
- [17] J. T. Babauta, H. D. Nguyen, T. D. Harrington, R. Renslow, H. Beyenal, *Biotechnol. Bioeng.* **2013**, *109*, 2651–2662.
- [18] D. Sun, S. Cheng, F. Zhang, B. E. Logan, *J. Power Sources* **2017**, *356*, 566–571.
- [19] B. Ranjan, J. Sim, H. Ryu, H. Ren, J. W. Santo, J. Chae, H. Lee, *Water Res.* **2017**, *127*, 230–238.
- [20] G. Yang, Q. Mai, Z. Zhuang, L. Zhuang, *Environ. Res.* **2021**, *201*, 111572.
- [21] J. Jo, A. Price-Whelan, L. Dietrich, *Nat. Rev. Microbiol.* **2022**, *20*, 593–607.
- [22] M. Atasoy, O. Eyice, A. Schnürer, Z. Cetecioglu, *Bioresour. Technol.* **2019**, *292*, 121889.
- [23] G. Yang, L. Huang, Z. Yu, X. Liu, S. Chen, *Water Res.* **2019**, *159*, 294–301.
- [24] J. Guo, G. Yang, Z. Zhuang, Q. Mai, L. Zhuang, *Sci. Total Environ.* **2021**, *797*, 149207.
- [25] T. Li, Q. Zhou, L. Zhou, Y. Yan, C. Liao, L. Wan, J. An, N. Li, X. Wang, *Water Res.* **2020**, *177*, 115776.
- [26] S. Pinck, L. M. Ostorumjof, S. Teychené, B. Erable, *Microorganisms* **2020**, *8*, 1841.
- [27] D. Salvatore, C. Bragato, *Environmental analysis by electrochemical sensors and biosensors*. Nanostructure Science and Technology. Springer, New York, **2014**, pp. 373–401.
- [28] D. Pocaznoi, B. Erable, M. L. Delia, A. Bergel, *Energy Environ. Sci.* **2012**, *5*, 5287–5296.
- [29] R. Rousseau, X. Dominguez-Benetton, M. L. Délia, A. Bergel, *Electrochem. Commun.* **2013**, *33*, 1–4.
- [30] P. Chong, B. Erable, A. Bergel, *Int. J. Hydrogen Energy* **2018**, *44*, 4484–4495.
- [31] K. P. Katuri, P. Kavanagh, S. Rengaraj, D. Leech, *Chem. Commun.* **2010**, *46*, 4758–4760.
- [32] E. Marsili, J. Sun, D. R. Bond, *Electroanalysis* **2010**, *22*, 865–874.
- [33] M. Rimboud, E. D. Quemener, B. Erable, A. Bergel, M. Rimboud, E. D. Quemener, B. Erable, T. Bouchez, A. Bergel, *Bioresour. Technol.* **2016**, *195*, 162–169.
- [34] K. P. Nevin, H. Richter, S. F. Covalla, J. P. Johnson, T. L. Woodard, A. L. Orloff, H. Jia, M. Zhang, D. R. Lovley, *Environ. Microbiol.* **2008**, *10*, 2505–2514.
- [35] G. D. Schrott, M. V. Ordoñez, L. Robuschi, J. P. Busalmen, *ChemSusChem* **2014**, *7*, 598–603.
- [36] D. Sun, S. Cheng, A. Wang, F. Li, B. E. Logan, K. Cen, *Environ. Sci. Technol.* **2015**, *49*, 5227–5235.
- [37] L. Karygianni, Z. Ren, H. Koo, T. Thurnheer, *Trends Microbiol.* **2020**, *28*, 668–681.
- [38] B. Cao, L. Shi, R. N. Brown, Y. Xiong, J. K. Fredrickson, M. F. Romine, M. J. Marshall, M. S. Lipton, H. Beyenal, *Environ. Microbiol.* **2011**, *13*, 1018–1031.
- [39] S. W. Li, G. P. Sheng, Y. Y. Cheng, H. Q. Yu, *Sci. Rep.* **2016**, *6*, 1–7.
- [40] A. P. Borole, G. Reguera, B. Ringeisen, Z. W. Wang, Y. Feng, B. H. Kim, *Energy Environ. Sci.* **2011**, *4*, 4813–4834.
- [41] J. B. Rollefson, C. S. Stephen, M. Tien, D. R. Bond, *J. Bacteriol.* **2011**, *193*, 1023–1033.
- [42] J. Wang, G. Li, H. Yin, T. An, *Environ. Res.* **2020**, *185*, 109451.
- [43] B. Erable, M.-A. Roncato, W. Achouak, A. Bergel, *Environ. Sci. Technol.* **2009**, *43*, 3194–3199.
- [44] M. Rimboud, L. Etcheverry, M. Barakat, W. Achouak, A. Bergel, *Bioresour. Technol.* **2021**, *337*, 125448.
- [45] R. Tapia-Tussell, R. E. Valle-Gough, I. Peraza-Baeza, J. Domínguez-Maldonado, M. Gonzalez-Muñoz, A. Cortes-Velazquez, R. M. Leal-Baustista, L. Alzate-Gaviria, *Sci. Total Environ.* **2019**, *681*, 258–266.
- [46] H. Kim, Y. J. Choo, J. Song, J. S. Lee, K. C. Lee, J. C. Cho, *Int. J. Syst. Evol. Microbiol.* **2007**, *57*, 1659–1662.
- [47] V. Fedorovich, M. C. Knighton, E. Pagaling, F. B. Ward, A. Free, I. Goryanin, *Appl. Environ. Microbiol.* **2009**, *75*, 7326–7334.
- [48] M. T. Fera, T. L. Maugeri, C. Gugliandolo, C. Beninati, M. Giannone, E. La Camera, M. Carbone, E. Marina, *Appl. Environ. Microbiol.* **2004**, *70*, 1271–1276.
- [49] S. Li, K. H. Nealson, **2015**, DOI 10.3389/fmicb.2015.00111.
- [50] A. G. Pereira-Medrano, M. Knighton, G. J. S. Fowler, Z. Yen, T. Khoa, S. Yen, A. Free, B. Ward, P. C. Wright, *J. Proteomics* **2012**, *78*, 197–210.
- [51] R. Askri, B. Erable, M. Neifar, L. Etcheverry, A. S. Masmoudi, A. Cherif, H. Chouchane, *Bioelectrochemistry* **2019**, *129*, 179–188.

- [52] R. Rousseau, C. Santaella, W. Achouak, J. J. Godon, A. Bonnafous, A. Bergel, M. L. Délia, *ChemElectroChem* **2014**, *1*, 1966–1975.
- [53] B. Thamdrup, R. Rosselló-Mora, R. Amann, *Appl. Environ. Microbiol.* **2000**, *66*, 2888–2897.
- [54] N. Pfennig, H. Biebl, *Arch. Microbiol.* **1976**, *110*, 3–12.
- [55] M. Pierra, A. A. Carmona-Martínez, E. Trably, J. Godon, N. Bernet, *Bioelectrochemistry* **2015**, *106*, 221–225.
- [56] E. Marsili, D. B. Baron, I. D. Shikhare, D. Coursolle, J. A. Gralnick, D. R. Bond, *Proc. Natl. Acad. Sci. USA* **2008**, *105*, 3968–3973.
- [57] D. R. Bond, D. R. Lovley, *Appl. Environ. Microbiol.* **2003**, *69*, 1548–1555.
- [58] E. Bolyen, J. R. Rideout, M. R. Dillon, N. A. Bokulich, C. C. Abnet, G. A. Al-Ghalith, H. Alexander, E. J. Alm, M. Arumugam, F. Asnicar, Y. Bai, J. E. Bisanz, K. Bittinger, A. Brejnrod, C. J. Brislawn, C. T. Brown, B. J. Callahan, A. M. Caraballo-Rodríguez, J. Chase, E. K. Cope, R. Da Silva, C. Diener, P. C. Dorrestein, G. M. Douglas, D. M. Durall, C. Duvallet, C. F. Edwardson, M. Ernst, M. Estaki, J. Fouquier, J. M. Gauglitz, S. M. Gibbons, D. L. Gibson, A. Gonzalez, K. Gorlick, J. Guo, B. Hillmann, S. Holmes, H. Holste, C. Huttenhower, G. A. Huttley, S. Janssen, A. K. Jarmusch, L. Jiang, B. D. Kaehler, K. Bin Kang, C. R. Keefe, P. Keim, S. T. Kelley, D. Knights, I. Koester, T. Kosciulek, J. Kreps, M. G. I. Langille, J. Lee, R. Ley, Y. X. Liu, E. Loftfield, C. Lozupone, M. Maher, C. Marotz, B. D. Martin, D. McDonald, L. J. McIver, A. V. Melnik, J. L. Metcalf, S. C. Morgan, J. T. Morton, A. T. Naimy, J. A. Navas-Molina, L. F. Nothias, S. B. Orchanian, T. Pearson, S. L. Peoples, D. Petras, M. L. Preuss, E. Pruesse, L. B. Rasmussen, A. Rivers, M. S. Robeson, P. Rosenthal, N. Segata, M. Shaffer, A. Shiffer, R. Sinha, S. J. Song, J. R. Spear, A. D. Swafford, L. R. Thompson, P. J. Torres, P. Trinh, A. Tripathi, P. J. Turnbaugh, S. Ul-Hasan, J. J. J. van der Hooft, F. Vargas, Y. Vázquez-Baeza, E. Vogtmann, M. von Hippel, W. Walters, Y. Wan, M. Wang, J. Warren, K. C. Weber, C. H. D. Williamson, A. D. Willis, Z. Z. Xu, J. R. Zaneveld, Y. Zhang, Q. Zhu, R. Knight, J. G. Caporaso, *Nat. Biotechnol.* **2019**, *37*, 852–857.
- [59] B. J. Callahan, P. J. McMurdie, M. J. Rosen, A. W. Han, A. J. A. Johnson, S. P. Holmes, *Nat. Methods* **2016**, *13*, 581–583.
- [60] K. Katoh, D. M. Standley, *Mol. Biol. Evol.* **2013**, *30*, 772–780.
- [61] M. N. Price, P. S. Dehal, A. P. Arkin, *Mol. Biol. Evol.* **2009**, *26*, 1641–1650.
- [62] D. McDonald, M. N. Price, J. Goodrich, E. P. Nawrocki, T. Z. Desantis, A. Probst, G. L. Andersen, R. Knight, P. Hugenholtz, *ISME J.* **2012**, *6*, 610–618.
- [63] L. Beule, P. Karlovsky, *PeerJ* **2020**, *8*, DOI 10.7717/peerj.9593.

Manuscript received: December 6, 2022

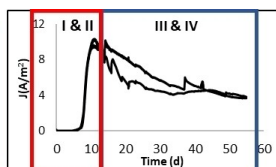
Revised manuscript received: February 17, 2023

Version of record online: ■■■■■

RESEARCH ARTICLE

Phases I & II

- ✓ Maximum current density
- ✓ High rate biofilm growth
- ✓ Higher microbial viability
- ✓ Maximum protein EPS content
- ✓ *Marinobacterium* spp.



Phases III & IV

- ✓ ~ 50% Current drop
- ✓ Biofilm growth rate declined
- ✓ Higher microbial mortality
- ✓ Decrease of EPS vs. microbial cells
- ✓ *Desulfuromonas* spp.

Typical electrochemical behaviour (middle graph) of microbial anodes is investigated when salt marsh electroactive biofilms (EABs) were formed on stainless steel microelectrodes. Maximum current dropped by more

than 50% after the peak. The main results found for before (phases I and II) the maximum current peak and after (phases III and IV) were summarized at both sides of the graph.

*L. Martinez Ostormujof, Dr. S. Teychené, Dr. W. Achouak, S. Fochesato, M. Bakarat, Dr. I. Rodriguez-Ruiz, Dr. A. Bergel, Dr. B. Erable**

1 – 14

Systemic Analysis of the Spatio-temporal Changes in Multi-Species Electroactive Biofilms to Clarify the Gradual Decline of Current Generation in Microbial Anodes

